Spectrum of Engineering Sciences
ISSN (e) 3007-3138 (p) 3007-312X Volume 4, Issue 4, 2026

ASSESSING THE IMPACT OF GEOLOGICAL VARIABILITY ON TUNNEL STABILITY: SENSITIVITY ANALYSIS OF THE KOHAT TUNNEL, PAKISTAN

[*1]Zahid Ur Rehman,[2]Mehreen Arif, [3]Faryal Rafique Khattak,[4]Sajjad Hussain, [5]Faizan Ali, [6]Muhammad Salman, [7]Arshad Ali

[*1]Department of Mining Engineering, University of Engineering and Technology, Peshawar, Pakistan.
[2]Department of Mining Engineering, University of Engineering and Technology, Peshawar, Pakistan.
[3]Department of Mining Engineering, University of Engineering and Technology, Peshawar, Pakistan.
[4]Department of Mining Engineering, University of Engineering and Technology, Peshawar, Pakistan.
[5]Department of Mining Engineering, University of Engineering and Technology, Peshawar, Pakistan.
[6]Department of Civil Engineering, University of Engineering and Technology, Peshawar, Pakistan.
[7]Department of Agricultural Engineering, University of Engineering and Technology, Peshawar, Pakistan.
[*1]engr.zahid@uetpeshawar.edu.pk

Keywords
Tunnel stability, geological variability, finite element modeling, RS2, Kohat Tunnel, Grey correlation method.

Article History
Received on 01 April, 2026
Accepted on 26 April, 2026
Published on 28 April, 2026

Corresponding Author:
Zahid Ur Rehman

Abstract

This research aims to evaluate the influence of geological heterogeneity on the tunnel stability and to determine the most sensitive rock mass parameters affecting structural performance, using the Kohat Tunnel in Pakistan as a case study. This study establishes a quantitative relationship between geological variability and tunnel stability through the integration of finite element modeling and Grey Correlation analysis, providing a structured framework for evaluating parameter sensitivity in heterogeneous rock masses. Finite element modeling was performed using RS2 software to stimulate the response of varying rock mass conditions along the tunnel alignment. Three geotechnical units -limestone ,sandy limestone, and shale -were modeled to analyze deformation behavior, stress redistribution, and Factor of Safety (FOS). A sensitivity analysis based on the Grey Correlation Method was conducted to quantify the relative influence of key geomechanical parameters on tunnel stability. The results indicate that the Geological Strength Index (GSI) are the dominant parameters controlling tunnel stability, with the correlation degree of 0.889 and 0.833, respectively. In contrast, Poisson's ratio and Young's modulus exhibit comparatively minor influence on the Factor of Safety. The analysis demonstrates that geological variability significantly alters stress distribution patterns and deformation characteristics within the tunnel surrounding rock mass. The findings support the development of more reliable and cost-effective tunnel support designs by prioritizing critical geomechanical parameters during site investigation and modeling. The proposed approach can be applied to tunnel projects in complex geological environments to improve stability prediction and risk mitigation strategies.

1. Introduction

Tunnels serve as critical elements within infrastructure networks, facilitating underground routes for transportation, utilities, and mining operations, which are essential to urban development and economic growth [1]. The performance and stability of tunnels are fundamentally influenced by the geological environment in which they are constructed, as the geological variability arising from natural sedimentation, tectonic activity, and erosion processes results in complex rock mass conditions [2]. Such variability manifests in spatial changes in lithology, joint orientation, groundwater presence, and strength properties, all of which significantly influence stress distribution and deformation behavior in tunnels [3]. Neglecting this variability can lead to costly design errors, excessive deformations, or catastrophic failures, highlighting the imperative for thorough geological characterization and risk assessment in tunnel engineering [4], [5].

Empirical approaches such as the Rock Mass Rating (RMR), Q-System, and Geological Strength Index (GSI) have been extensively applied during the preliminary stages of tunnel design due to their practical correlations between rock mass parameters and tunnel stability [6]. However, these systems typically exhibit deterministic limitations that restrict their Tunnels represent essential components of modern infrastructure systems, providing critical underground pathways for transportation networks, utility conduits, and mining activities. Their role is increasingly significant in facilitating urbanization, economic development, and connectivity, especially in challenging terrains where surface routes are limited or congested [17]. The safety, functionality, and longevity of tunnels are intricately linked to the geological environments through which they are excavated. Geological variability, caused by natural processes such as sedimentation, tectonic deformation, weathering, and erosion, leads to complex rock mass conditions characterized by heterogeneous lithology, discontinuities, varying groundwater conditions, and diverse mechanical properties. These factors fundamentally influence stress redistribution, deformation patterns, and failure mechanisms around tunnels [18],[31]. Failure to capability to encompass the complexities of real geological environments, including heterogeneity and anisotropy [7]. Instead, numerical methods, particularly finite element modeling (FEM), have become prominent robust tools enabling detailed analysis of the interaction between rock mass and excavation processes [8]. FEM facilitates evaluation of stress redistribution, plastic deformation, and support performance across varying geological scenarios, thereby enhancing the predictive capacity of tunnel stability assessments [9]. The present study uses RS2 software, a two-dimensional FEM platform developed by Rocscience, to simulate tunnel stability under variable geological conditions characteristic of the Kohat Tunnel in Khyber Pakhtunkhwa, Pakistan a region marked by heterogeneous rock mass composition [10]. The study objectives include comprehensive rock mass classification, simulation of diverse geological scenarios, and implementation of sensitivity analysis via the Grey Correlation Method to elucidate dominant factors impacting tunnel stability. Enhanced understanding of geological variability through these approaches aims to foster improved tunnel design methodologies that better accommodate complex subsurface conditions, thereby optimizing safety and performance [11], [12].

adequately account for such variability can result in inaccurate design assumptions, excessive ground movements, increased support demands, cost overruns, and in severe cases, catastrophic structural failures [19],[30].

Traditional empirical methods such as Rock Mass Rating (RMR), Q-System, and Geological Strength Index (GSI) have been widely adopted for initial rock mass characterization and rapid stability assessments. These tools provide valuable, practical correlations between rock mass conditions and support requirements that guide preliminary design decisions [20]. However, the inherently deterministic nature of these empirical systems limits their ability to capture the full complexity and spatial variability of geological conditions encountered in practice [21]. This shortcoming has driven the adoption of advanced numerical modeling techniques, with finite element modeling (FEM) emerging as a

robust and versatile approach to simulating tunnel excavation and rock–support interaction [22][32]. FEM enables detailed assessment of stress redistribution, plastic deformations, potential failure zones, and support system performance, incorporating diverse geological scenarios and mechanical behaviors, which improves predictive accuracy and design optimization [23][33-38].

In this context, the present study employs RS2 software an established two-dimensional finite element modeling platform offered by Rocscience to investigate tunnel stability under variable geological conditions. The Kohat Tunnel in Pakistan, characterized by a heterogeneous rock mass composition due to alternating lithologies and complex structural geology, serves as a representative case study [24][25]. The objectives encompass detailed rock mass classification using empirical indices, simulation of multiple geological scenarios affecting tunnel behavior, and sensitivity analysis employing the Grey Correlation Method to identify key factors driving stability outcomes. Through this multifaceted approach, the study aims to quantify the impact of geological variability on tunnel performance and provide insights that enhance design practices by integrating empirical and numerical modeling frameworks [25], [26-38].

Advances in geological detection technologies, including ahead geological detection and real-time monitoring during excavation, increasingly complement empirical and numerical methods by offering dynamic, non-invasive insight into subsurface conditions. These integrated approaches facilitate proactive risk management and adaptive construction strategies, which are crucial for navigating complex geological environments such as those encountered in the Kohat Tunnel project [26], [27]. This research contributes to the growing body of knowledge that underscores the necessity of comprehensive geological characterization combined with sophisticated modeling tools to achieve safer, cost-effective, and resilient tunnel designs [28], [29-36].

Thus, by integrating empirical rock mass classifications, numerical modeling via FEM, and sensitivity analyses, the study endeavors to establish a robust framework for addressing geological variability in tunnel engineering, ultimately enhancing the predictability and reliability of underground construction projects.

2. Geological Characterization and Integrated Data of the Kohat Tunnel

The Kohat Tunnel is situated within the geologically complex terrain of the Kohat Pass, Khyber Pakhtunkhwa, Pakistan, where the tunnel alignment traverses interbedded sedimentary sequences of limestone, sandy limestone, and shale belonging to the Jurassic–Cretaceous formations. These lithological units exhibit pronounced heterogeneity in their physical and mechanical properties, primarily controlled by depositional environments, tectonic deformation, and varying degrees of weathering.

The limestone unit (GTU-I) is predominantly massive and relatively competent, with moderate jointing and comparatively higher uniaxial compressive strength and Geological Strength Index (GSI) values. This unit generally provides favorable ground conditions, capable of sustaining in-situ and excavation-induced stresses with limited deformation. In contrast, the sandy limestone unit (GTU-II) exhibits moderate weathering, variable bedding characteristics, and irregular joint spacing. These features impart intermediate strength and deformability, resulting in a heterogeneous mechanical response that necessitates careful consideration in design and analysis.

The shale unit (GTU-III) represents the weakest and most problematic lithology along the tunnel alignment. It is highly fractured, weak, and susceptible to time-dependent deformation and squeezing under elevated stress conditions. The significantly lower strength and stiffness of shale, combined with its anisotropic behavior, pose substantial challenges for tunnel stability and require robust and immediate support measures during excavation.

A comprehensive geotechnical investigation program was undertaken, including core drilling, detailed geological mapping, and laboratory testing of representative rock samples. These investigations provided essential data on key physical and mechanical properties such as density, porosity, uniaxial compressive strength (UCS), tensile strength, and elastic modulus. The

resulting dataset enabled reliable rock mass classification and served as a critical input for both empirical design approaches and advanced numerical modeling.

The tunnel overburden ranges from approximately 150 to 200 meters, placing the excavation within a shallow-to-intermediate depth regime. This overburden significantly influences the stress conditions and contributes to spatial variability in rock mass behavior. Furthermore, the presence of discontinuities such as joints, bedding planes, and potential groundwater ingress adds complexity to the stress redistribution and deformation patterns around the excavation.

Overall, the pronounced geological variability across the three geotechnical units governs the mechanical response of the rock mass and plays a decisive role in tunnel stability. Accurate representation of this heterogeneity through integrated geological characterization, laboratory testing, and numerical modeling is essential for the safe and efficient design of the Kohat Tunnel. The marked contrast in strength and deformability, particularly between limestone and shale units, underscores the necessity for adaptive support systems and detailed sensitivity analyses to address the challenges associated with tunneling in complex and variable ground conditions. The different integrated data of rock masses along the Kohat tunnel is presented in Table 1.2.

Table 1: *Geological Characterization and Integrated Data of the Kohat Tunnel*

S.No	Parameter	Limestone			Sandy Limestone			Shale		
		Min	Max	Avg.	Min	Max	Avg.	Min	Max	Avg.
1	Unit weight, γ (KN/m3)	26.20	27.20	26.70	25.20	27.20	26.40	25.30	26.80	25.90
2	Uniaxial Compressive Strength, σc (MPa)	52.20	62.20	57.20	25.60	48.90	37.80	3.66	9.80	6.73
3	Uniaxial tensile Strength, σt (MPa)	6.79	7.99	8.90	3.41	6.45	4.98	-	-	-
4	Modulus of elasticity, E (GPa)	15.20	29.00	22.10	7.50	15.20	11.40	0.10	1.93	0.72
5	Poisson"s ratio, υ	0.20	0.30	0.27	0.26	0.34	0.30	0.29	0.35	0.32
6	Hoek – Brown Constant, mi	8.00			6.00			6.00 ±2		

2.3 Stress Conditions along the alignment of Kohat tunnel

The magnitude of horizontal and vertical stresses along the alignment of the Kohat Tunnel demonstrates significant variation depending on the lithology of the rock formations through which the tunnel passes. According to Table 6, the limestone (CI) and sandy limestone (CII) formations are characterized by relatively low vertical and horizontal stresses. Specifically, the vertical stresses in limestone and sandy limestone are 2.14 MPa and 1.58 MPa, respectively, while the horizontal stresses are correspondingly 0.79 MPa and 0.68 MPa. These lower stress levels indicate that these rock types are comparatively more resistant and less deformable under the existing geostatic conditions.

In contrast, the shale formation (DI) along the Kohat Tunnel alignment exhibits significantly higher stress magnitudes, with vertical stress reaching 7.90 MPa and horizontal stresses measured at 3.72 MPa. These elevated stress values suggest that shale is a weaker and more deformable rock type, prone to greater deformation and potential instability under tunneling loads. The contrast in stress magnitudes between the limestone/sandy limestone and shale formations underscores the importance of lithological variations in influencing the in-situ stress distribution and the geotechnical behavior of the tunnel alignment.

Furthermore, the stress ratio K, defined as the ratio of horizontal to vertical stress, ranges from 0.37 to 0.47 along the tunnel. This relatively low ratio indicates a gravity-dominated stress regime where the vertical stress component due to the weight of the overburden is more significant than horizontal tectonic stresses. Such a stress regime suggests that the tunnel's stability and design primarily need to consider vertical loading effects, with horizontal stresses playing a secondary but still crucial role in rock mass behavior and support requirements.

These findings are consistent with principles of soil and rock mechanics that relate stress magnitudes to rock type and structural geology, influencing deformation and failure mechanisms in underground excavations. The differentiation of stress states across varying lithological units highlights the necessity to tailor engineering designs and reinforcement strategies according to localized stress variations to ensure tunnel safety and durability under operational conditions. The stress conditions along the tunnel axis is presented in Table 2.

Table 2: ***Stress Conditions along the alignment of Kohat tunnel***

GTU	Rock type	Vertical Stress (MPa)	Horizontal Stress (MPa)	K
CI	Limestone	2.14	0.79	0.37
CII	Sandy limestone	1.58	0.68	0.43
DI	Shale	7.90	3.72	0.47

2.4 Strength Parameters of Rock Mass Along the alignment of Kohat tunnel

The laboratory-derived strength parameters and Hoek–Brown constants for limestone, weathered limestone, and shale reveal a significant variability in the mechanical behavior of the rock masses encountered along the Kohat Tunnel alignment. This variability has direct implications for tunnel stability, excavation performance, and support design in a mining and tunneling context.

The intact limestone exhibits comparatively higher uniaxial compressive strength (σc = 9.785 MPa) and tensile strength (σt = 0.273 MPa), along with higher Hoek–Brown constants (mb = 1.785, s = 0.094, a = 0.503). These values indicate a relatively competent rock mass with moderate strength and better interlocking characteristics. However, the strength values still fall within the range of weak to moderately weak rock, suggesting that even intact limestone in the Kohat Tunnel is not exceptionally strong and may be susceptible to deformation under high in-situ stresses.

In contrast, the weathered limestone shows a substantial reduction in both compressive (σc = 3.636 MPa) and tensile strength (σt = 0.047 MPa), accompanied by a sharp decrease in the Hoek–Brown parameter s (0.0007). This reduction reflects the effects of weathering, which leads to the degradation of bonding, increased porosity, and the development of

micro-fractures. The lower mb value (0.589) further indicates reduced frictional strength and inter-particle resistance. Such conditions are critical in tunneling, as weathered zones are likely to behave as weak strata, contributing to localized instability, overbreak, and the need for immediate support.

The shale unit represents the weakest material encountered, with extremely low compressive strength (σc = 0.404 MPa) and tensile strength (σt = 0.004 MPa). The Hoek–Brown parameters (mb = 0.308, s = 0.0002, a = 0.538) confirm its very poor rock mass quality. The very low s value indicates a highly fractured or structurally disturbed material, while the low mb suggests minimal shear strength. In the context of the Kohat Tunnel, shale layers are expected to behave in a ductile to highly deformable manner, making them prone to squeezing, slaking, and time-dependent deformation. These characteristics significantly increase the risk of tunnel convergence and instability, particularly under high overburden stresses.

Overall, the results highlight a high degree of geological variability, ranging from relatively competent limestone to extremely weak shale. This heterogeneity plays a crucial role in governing tunnel stability and must be carefully incorporated into numerical modeling and sensitivity analysis. The transition zones between limestone and weaker units (weathered limestone and shale) are particularly critical, as they may act as zones of stress concentration and differential deformation. The different Strength and Hoek–Brown Parameters are presented in Table 3.

Table 3: ***Strength and Hoek–Browns Parameters of Rock Mass Along the Axis of Kohat Tunn Rock Mass Classification and Support Recommendations for Rock mass Along the Alignment of Kohat Tunnel using RMR***

S.No	Rock Type	Strength Parameters		Hoek–Brown Parameters		
		σ_c (MPa)	σ_t (MPa)	M_b	S	a
1	Limestone	9.785	0.273	1.785	0.094	0.503
2	Limestone weathered	3.636	0.047	0.589	0.0007	0.516
3	Shale	0.404	0.004	0.308	0.0002	0.538

The Rock Mass Rating (RMR) system offers a well-established, empirical framework to systematically select appropriate support measures for tunnel excavation based on the varying quality of rock masses encountered along the Kohat Tunnel alignment. This approach ensures that excavation and reinforcement strategies are effectively tailored to the specific geotechnical conditions present at different stations, optimizing safety and construction efficacy. The details of the rock mass classes and support system recommended for each unit are presented in Table 4 and Table 5.

Table 5 shows: At stations 16+362 and 17+725, the rock mass is classified as good quality with RMR values ranging from 65 to 70. Such rock conditions allow for full-face excavation, minimizing disruptions to progress and costs. Support requirements under these conditions are limited, typically involving the installation of locally placed 3-meter rock bolts which provide sufficient reinforcement of the rock mass. Occasional wire mesh installation is adopted in areas susceptible to minor rock fall or spalling, ensuring additional safety without excessive use of materials or time

In contrast, station 17+996 presents fair rock mass quality characterized by an RMR of 42, indicating moderately fractured or weathered conditions warranting more cautious excavation methods. Here, staged excavation using a top heading and bench method is recommended to control excavation-induced stress redistribution carefully. Reinforcement consists of 4-meter fully grouted bolts installed at 1.5-2-meter spacing in the crown and walls, combined with 50-100 mm thick shotcrete lining for rock surface consolidation. Wire mesh installation in the crown further aids in controlling loose rock fragments, addressing the increased deformation potential in the rock mass.

At the weakest rock zone, station 17+314, the rock quality is assessed as poor with an RMR of 29. The highly fractured and weak rock in this segment necessitates intensive support measures to ensure excavation stability and worker safety. Support includes the installation of longer rock bolts of 4 to 5 meters in length at closer spacing

of 1 to 1.5 meters. Thicker shotcrete layers ranging from 100 to 500 mm are applied to the crown and sides to reinforce the excavation boundaries effectively. Such robust support controls excessive deformation and prevents collapse, exemplifying the critical influence of rock mass quality on support design density and type.

The direct correlation between the RMR classification and required support intensity highlights the vital role empirical systems like RMR play in underground excavation projects. It underscores the importance of detailed geological and geotechnical investigations to identify variable rock mass conditions along the tunnel and to design site-specific reinforcement strategies that balance safety, cost, and construction efficiency This tailored approach not only mitigates risks associated with variable geological conditions but also optimizes resource utilization during construction, helping to ensure long-term tunnel stability and operational success. In conclusion, the application of the RMR system along the Kohat Tunnel allows a rational and adaptable framework for support design, adjusting from minimal reinforcement in good quality rock to substantial support schemes in poor quality zones, thus harmonizing excavation techniques with the varying geotechnical environment. The various rock mass classes along the alignment of Kohat Tunnel and support requirements are summarized in Table 4 and Table 5.

Table 4: ***Rock mass classification along the tunnel axis using Basic RMR***

GTU	Rock type	Rock Mass Rating	Rock mass Class	Rock Mass Quality	GSI
CI	Limestone	65-70	II	Good rock	60-65
CII	Sandy Limestone	42	III	Fair rock	39
DI	Shale	29	IV	Poor rock	24

Table 5: ***RMR support Recommendations for Rock mass Along the of Kohat Tunnel***

Station	Rock Mass Class	Excavation	Rock bolts (fully grouted with 20 mm diameter)	Shotcrete	Steel set
STA 16+362	**RMR: 65** II – Good rock	Full face 1 – 1.5 m advance. Complete support 20 m from face	Locally, bolt in crown 3.0 m long, spaced 2.5 m with occasional wire mesh	50 mm in crown where required	None
STA 17+996	**RMR: 42** III – Fair rock	Top heading and bench 1.5 – 3 m advance in top heading. Commence support after each blast. Complete support 10 m from face.	Systematic bolts 4 m long, spaced 1.5 – 2 m in crown and walls with wire mesh in crown	50 – 100 mm in crown and 30 mm in side	None
STA 17+314	**RMR: 29** IV – Poor rock	Top heading and bench 1.0 – 1.5 m advance in top heading. Commence support after each blast. Complete support	Systematic bolts 4-5 m long, spaced 1.0 – 1.5 m in crown and walls with wire mesh	100 – 150 mm in crown and 100 mm in sides	Light to medium ribs spaces 1.5 m where required

		10 m from face.		
STA 16+725	**RMR: 70** II – Good rock	Full face 1 – 1.5 m advance. Complete supportwith 20 m from face	Locally, bolt in crown 350 mm m long, spaced 2.5 mcrown where occasional wirerequired mesh	inNone

3. Numerical Modelling

Finite Elements Analysis (FEA) was conducted using RS2 to evaluate the stability of the Kohat Tunnel under varying geological conditions. Three geological units (GTUs) were analyzed independently to isolate the influence of geological variability on tunnel behavior. Identical model geometry, boundary conditions, and analysis producers were applied to all GTUs so that observed differences in resources could be attributed solely to variations in rock mass properties. Rock mass behavior was simulated using the generalized Hoek-Brown constants (mb, s, and a), unit weight, Young's modulus, and Poisson's ratio to define both strength and deformation characteristics of the rock mass. These parameters were assigned directly from laboratory testing and rock mass classification results. The numerical model boundaries were defined following standard RS2 practice. Roller boundaries were applied along the vertical sides of the model to restrict horizontal displacement while allowing vertical movement. The base of the model was fully fixed to prevent both vertical and horizontal displacements. Initial in-situ stresses were generated using horizontal stress ratio, K= σ h / σ v, derived from field measurements , ensuring realistic pre-excavation stress conditions. The tunnel excavation was assumed to be circular and was simulated using staged excavation in RS2. Tunnel support was modeled using equivalent elastic liners to represent shotcrete, while rock bolt effects were incorporated through rather than discrete bolt elements. Excavation and support installation followed RMR-based recommendations for each geotechnical unit to reflect actual construction practices.

To assess the sensitivity of tunnel stability to key rock mass parameters, a parametric study was performed by varying Geological Strength Index (GSI), UCS, Young's modulus (E), and Poisson's ratio (v)by +−25% relative to their baseline values. The resulting Factors of Safety (FOS) obtained from RS2 were compared to evaluating parameter influence. The Grey Correlation Method (GCM) was then applied to quantity the relative contribution of each parameter to tunnel stability. The correlation of the sensitivity of FOS to each parameter, with higher values indicating greater influence.

To analyze the models developed in FEA software RS2, the following conventions were adopted.

1. Immediate support installation after excavation and enlargement.
2. Assuming Elasto-plastic behavior of rock mass with generalized Hoek-Brown criterion is adopted for models' simulations.
3. The model of the Tunnel is 2D by considering plane strain problem

3.1 Design Input Parameters for RS2 Modeling of GTU-1 (Limestone)

Numerical modeling for GTU-I, GTU-II, and GTU-III was carried out using RS2 finite element software based on the respective geotechnical input parameters. The results of the numerical simulations are summarized in Table 6. However, in this paper, only the input parameters and modeling setup for GTU-I (limestone) are presented and discussed in detail, while the modeling parameters for GTU-II and GTU-III are not included here for brevity. Table 6 summarizes the key geotechnical input parameters and support design adopted for numerical modeling of GTU-I (limestone) in RS2 software along the Kohat Tunnel alignment. The rock mass is characterized by a relatively high uniaxial compressive strength of 57.2 MPa, indicating moderately strong rock conditions. The high Young's modulus (22.1 GPa) and low Poisson's ratio (0.27) reflect a stiff and brittle mechanical response typical of competent limestone. The Generalized Hoek–Brown parameters (mb = 3.438, s = 0.0205, a = 0.502) indicate a moderately fractured but overall intact rock mass with limited degradation of strength. A unit weight of 26.7 kN/m³ (0.0267 MN/m³) was used to represent the self-weight of the rock mass in the numerical model. In-situ stress conditions

were incorporated through a horizontal-to-vertical stress ratio (K = 0.369), representing a stress regime dominated by vertical loading. This parameter plays a key role in defining stress redistribution and deformation patterns around the excavation boundary.

The support system was designed based on RMR classification (approximately Class II – good rock). Accordingly, a relatively light support scheme was adopted, including full-face excavation, 3 m long fully grouted rock bolts installed in the crown at 2.5 m spacing, wire mesh reinforcement, and a 50 mm thick layer of shotcrete in the crown. This support configuration reflects the self-supporting capacity of the limestone and is intended primarily for surface confinement and loosening control rather than heavy structural reinforcement.

Table 6: ***Design input parameters for RS2 modeling of GTU-1***

Uni-axial Compressive Strength (MPa)	Generalized Hoek-Brown constants			Unit weight (MN/m^3)	Poisson ratio	Young Modulus (MPa)	K
	Mb	s	a				
57.2	3.438	0.0205	0.502	0.0267	0.27	22100	0.369
	RMR Support						
Support System	**Excavation**	Full face					
	Bolt length	3m in crown with wire mesh					
	Bolt spacing	2.5 meter					
	Shotcrete	50mm thickness in crown					

These parameters were directly implemented in the RS2 numerical model to simulate excavation-induced stress redistribution and assess tunnel stability under limestone conditions. The results provide a realistic representation of rock mass behavior and clearly demonstrate the influence of rock quality on support intensity and deformation response along the tunnel alignment. The results of numerical modeling for GTU-I are shown in Figure 1.1 to 1.9.

Spectrum of Engineering Sciences
ISSN (e) 3007-3138 (p) 3007-312X
Volume 4, Issue 4, 2026

For GSI Variation

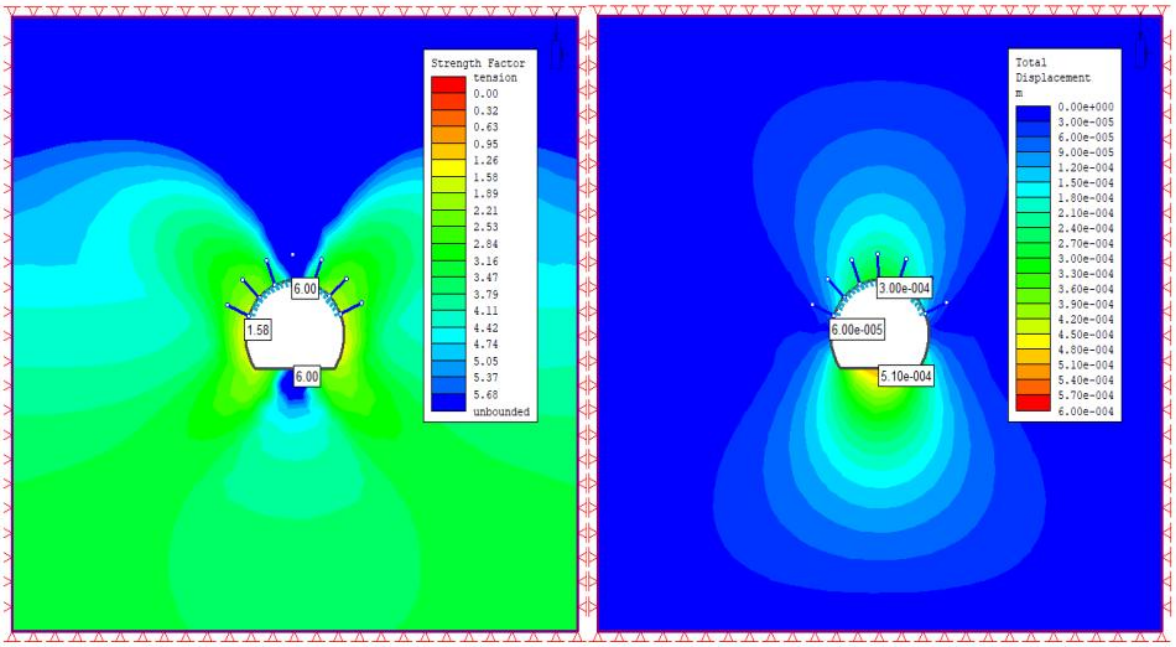

Figure 1.1 Simulated models for GTU-I (for actual baseline values of all parameters)

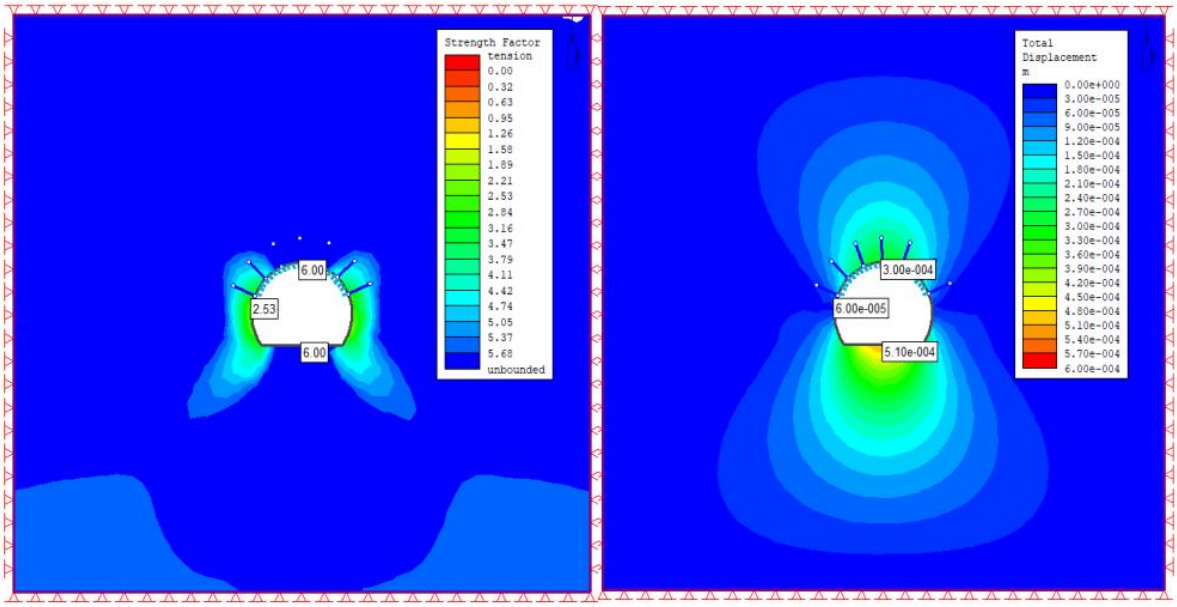

Figure 1.2 Simulated models for GTU-I (for 25% Increase in GSI Value)

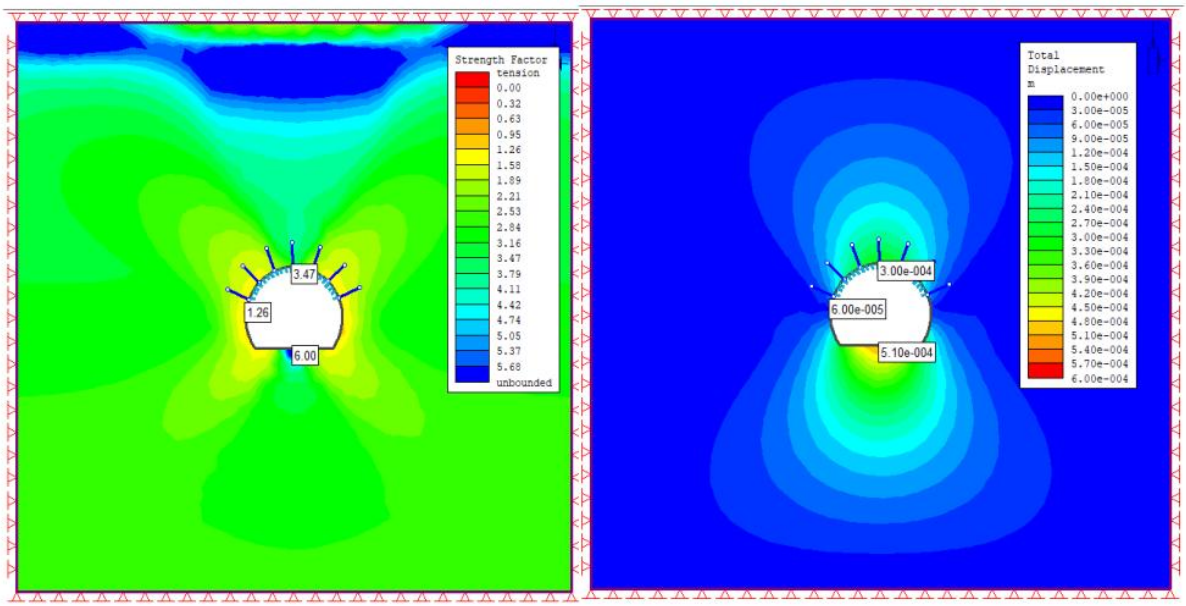

Figure 1.3 Simulated models for GTU-I (for 25% decrease in GSI Values)
For Poisson Ratio Variation

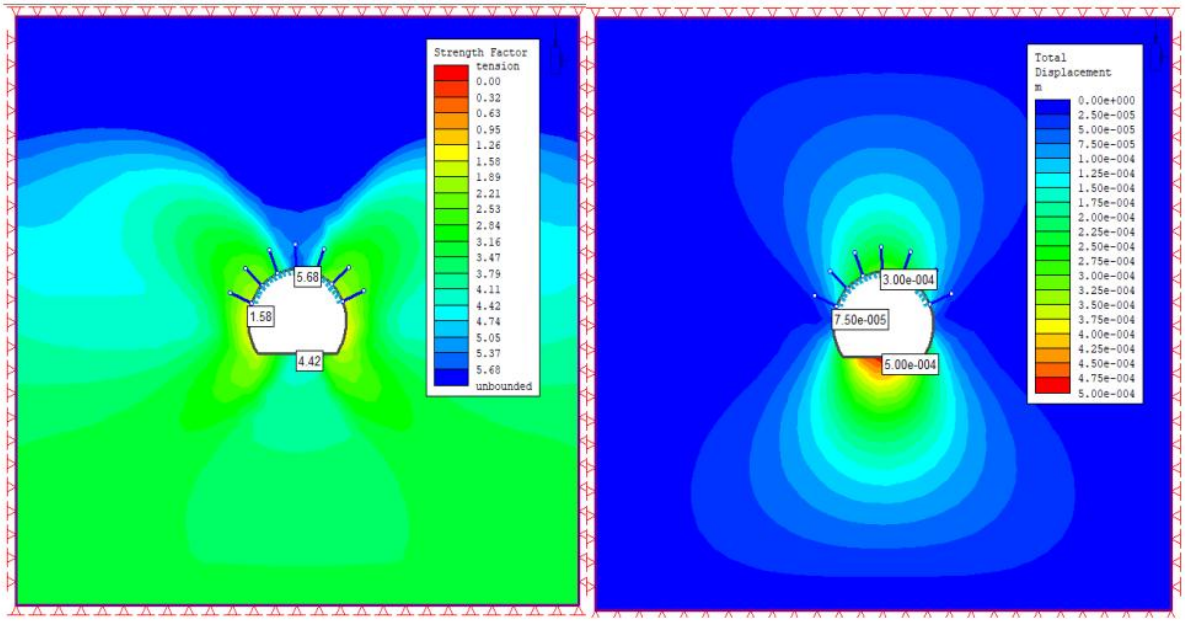

Figure 1.4 Simulated models for GTU-I (Poisson ratio 25% Increasing)

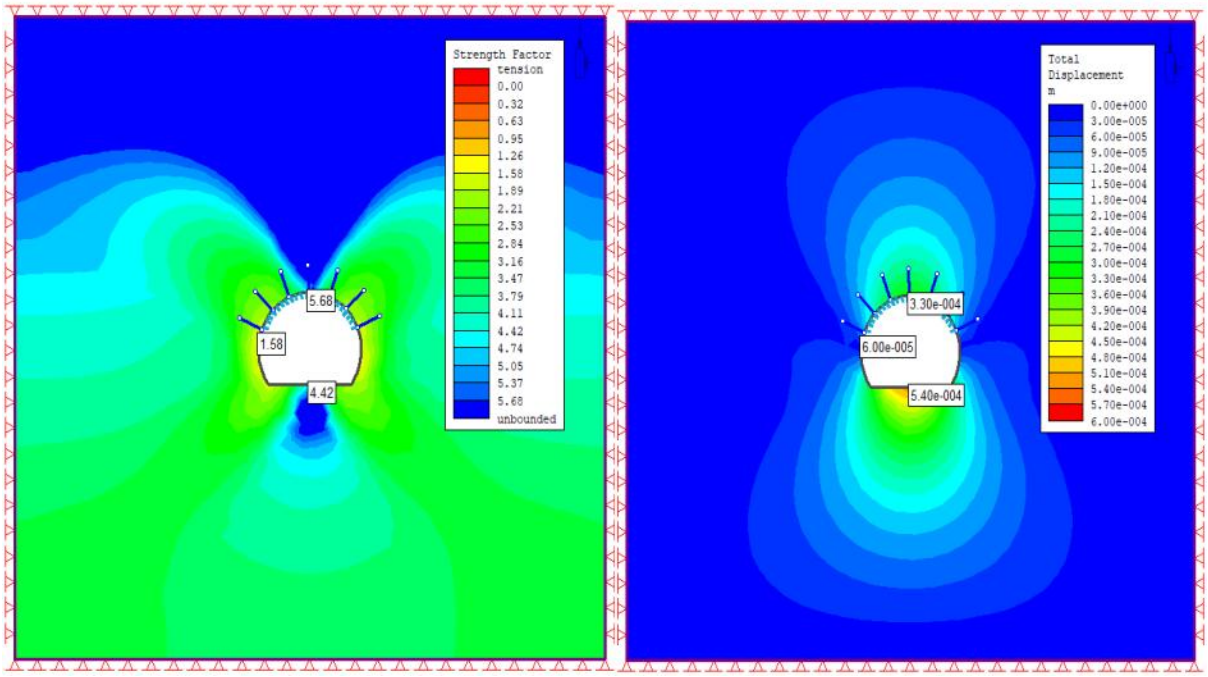

Figure 1.5 Simulated models for GTU-I (Poisson ratio 25% Decreasing

For UCS Variation

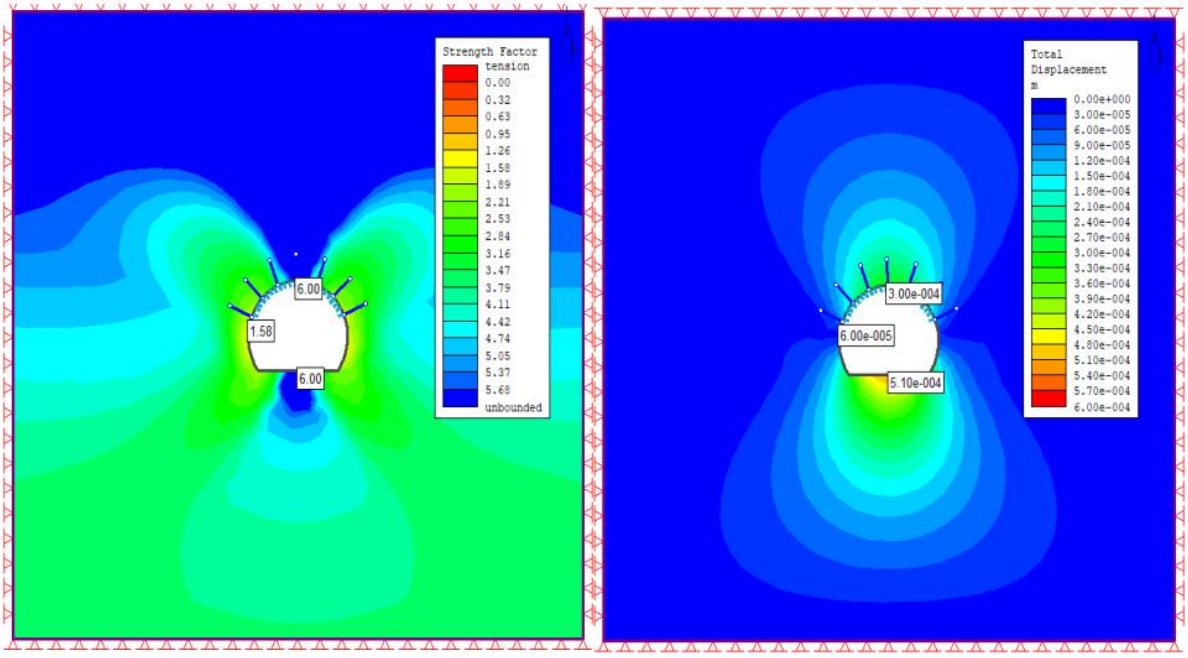

Figure 1.6 Simulated models for GTU-I (UCS 25% Increasing)

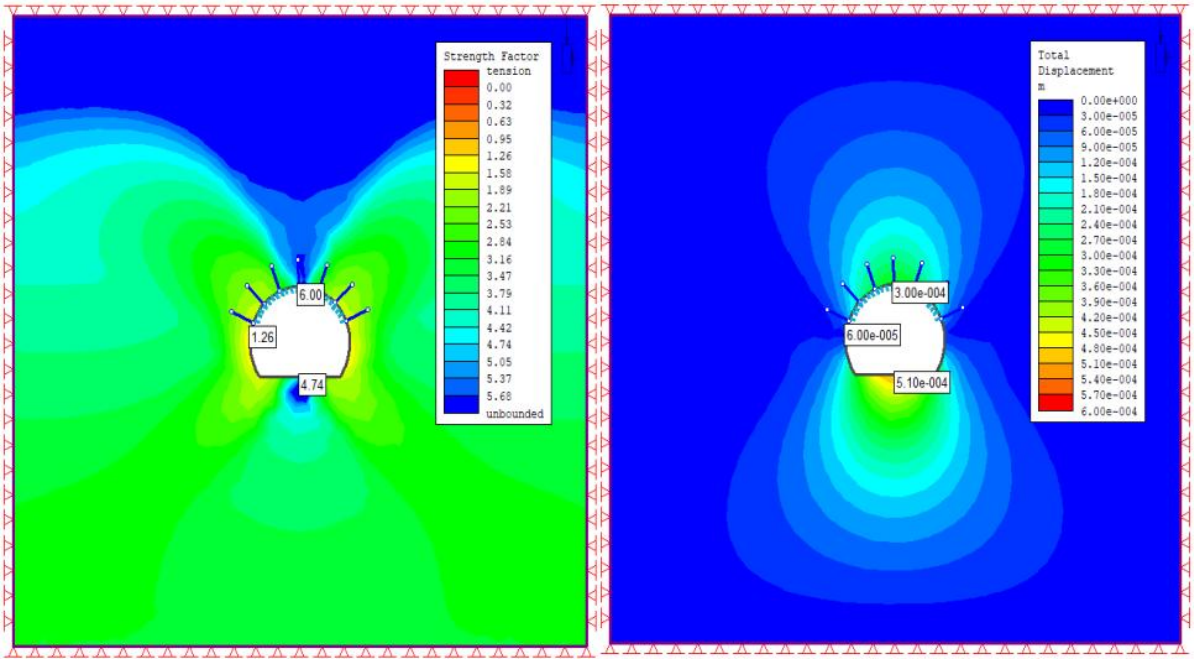

Figure 1.7 Simulated models for GTU-I (UCS 25% Decreasing)

For Young Modulus Variation

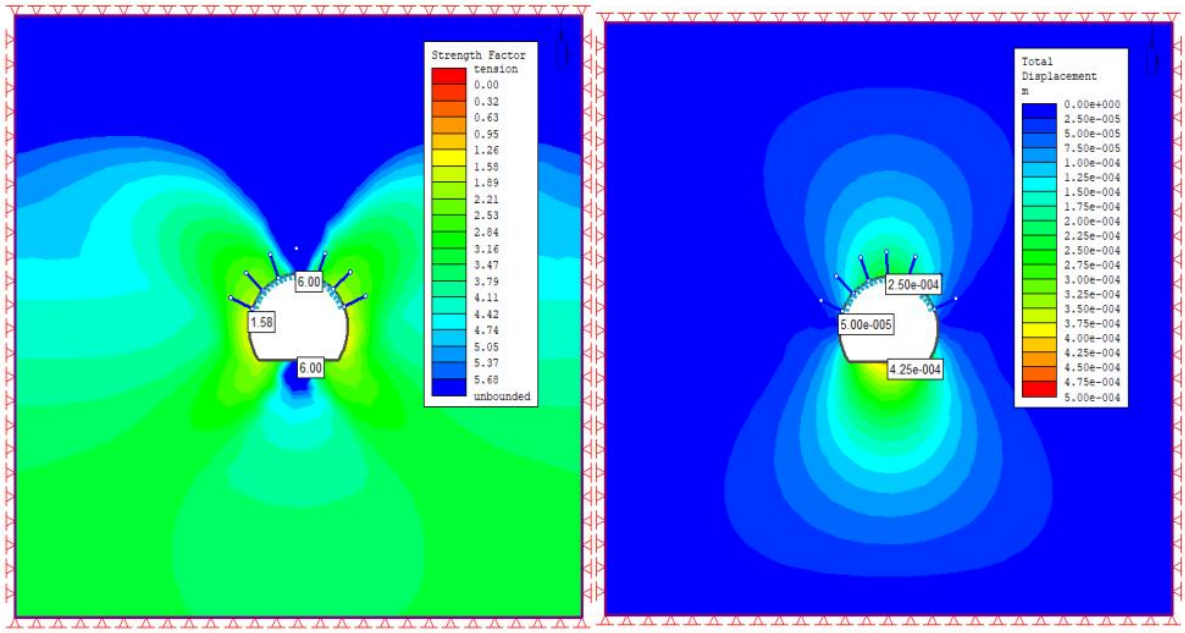

Figure 1.8 Simulated models for GTU-I (Young Modulus 25% Increasing

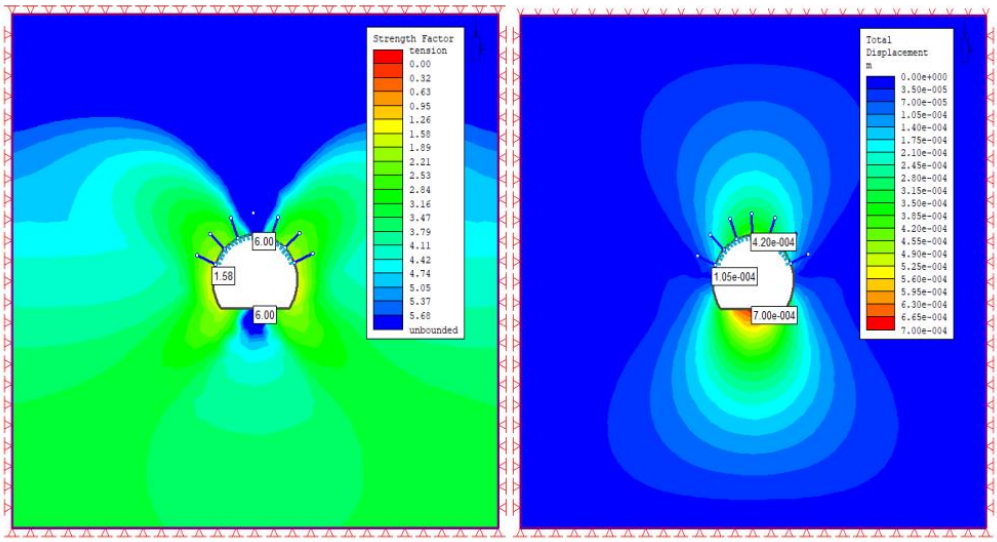

Figure 1.9 simulated models for GTU-I (Young Modulus 25% Decreasing)

3.2 Analysis of numerical models for different geotechnical units

The numerical modeling results clearly demonstrate significant variations in tunnel response across the three geotechnical units (GTU-I, GTU-II, and GTU-III), highlighting the strong influence of lithological variability on excavation stability. The different results obtained from numerical analysis are presented in Table 7 to Table . The limestone unit (GTU-I) exhibits the most stable performance due to its relatively high stiffness (Young's modulus of 22.1 GPa) and favorable rock mass strength parameters. As a result, deformation after excavation is minimal, and the rock mass effectively sustains the induced stresses. The computed strength factors are highest at the crown (6.00) and remain acceptable at the sidewall (1.58), indicating stable conditions with adequate safety margins. Correspondingly, total displacements are very low, with values of 0.30 mm at the crown and 0.06 mm at the sidewall, reflecting excellent self-supporting capacity of the limestone.

In contrast, the sandy limestone unit (GTU-II) exhibits intermediate behavior characterized by reduced stiffness and moderately weaker rock mass properties. This reduction in mechanical competence results in lower strength factors compared to limestone and a noticeable increase in deformation response. The computed displacements rise to 0.60 mm at the crown and 0.20 mm at the sidewall, indicating moderate stability conditions. Although the rock mass remains generally stable, its heterogeneous nature and variable jointing make it more sensitive to stress redistribution induced by excavation.

The shale unit (GTU-III), however, demonstrates the poorest mechanical performance among all units. Due to its very low stiffness, weak bonding, and highly fractured nature, it undergoes significant deformation following excavation. The crown displacement increases substantially to 2.25 mm, indicating a high potential for instability and localized failure zones. The low strength and deformability of shale make it highly susceptible to squeezing behavior, particularly under in-situ stress conditions, thereby necessitating immediate and robust support measures during tunneling.

Overall, the results confirm a strong correlation between rock mass strength/stiffness and tunnel stability response. As rock quality decreases from limestone to shale, there is a consistent reduction in strength factor and a corresponding increase in deformation. This trend clearly emphasizes that the mechanical behavior of the tunnel is governed primarily by lithological variability and rock mass condition, as summarized in Table 10. The findings further highlight the importance of incorporating realistic geotechnical parameters into numerical models to accurately predict deformation patterns and optimize support design in heterogeneous ground conditions

Table 7: *Analysis of numerical models for different geotechnical units (Actual base values)*

S.No	Rock type	Young Modulus (E) MPa	UCS MPa	GSI	Poisson ratio (V)	Generalized Hoek -Brown Parameters			Strength factor (F.O.S)		Total Displacement (mm)	
						mb	s	a	Crown	Sidewall	Crown	Sidewall
									After excavation		After excavation	
1	Limestone	22100	57.20	65.00	0.27	3.438	0.0205	0.502	6.00	1.58	0.30	0.06
2	Sandy Limestone	11400	37.80	39.00	0.30	1.641	0.0011	0.512	1.58	1.26	0.60	0.20
3	Shale	720	6.73	24.00	0.32	0.773	0.0002	0.533	2.84	1.26	6.75	2.25

Table 8: *Analysis of numerical models for different geotechnical units (for 25% Increase in GSI Values)*

S.No	Rock type	GSI	UCS MPa	Young Modulus (E) MPa	Poisson ratio (V)	Generalized Hoek -Brown Parameters			Strength factor Strength factor (F.O.S)		Total Displacement (mm)	
						mb	s	a	Crown	Sidewall	Crown	Sidewall
									After excavation		After excavation	
1	Limestone	81.25	57.2	22100	0.27	6.143	0.1245	0.501	6.00	2.53	0.30	0.06
2	Sandy Limestone	48.75	37.8	11400	0.30	2.325	0.0034	0.506	1.89	1.26	0.60	0.20
3	Shale	30	6.73	720	0.32	0.958	0.0004	0.522	2.84	1.26	6.75	2.25

Table 7 presents the analysis of numerical models for three geotechnical rock units—Limestone, Sandy Limestone, and Shale—based on their mechanical properties and excavation behavior. Limestone, with the highest Young's modulus (22,100 MPa), UCS (57.2 MPa), and GSI (65), shows the greatest stability, reflected by a high strength factor (6.00 at crown) and minimal displacement (0.30 mm at crown). Sandy Limestone, with moderate strength and stiffness, exhibits lower stability (strength factor 1.58) and moderate displacement (0.60 mm). In contrast, Shale, characterized by very low stiffness (720 MPa), strength (UCS 6.73 MPa), and GSI (24), demonstrates the poorest performance, with a low strength factor (2.84) and the highest total displacement (6.75 mm), indicating the need for extensive support in excavation. Overall, the results highlight that rock strength and quality significantly influence excavation stability and deformation.

Table 8 shows the effect of a 25% increase in Geological Strength Index (GSI) on the numerical model behavior of three rock types: Limestone, Sandy Limestone, and Shale. With the increased GSI values, all rocks exhibit improved Hoek-Brown parameters, especially mb and s, indicating enhanced rock mass strength. Limestone, with the highest GSI (81.25), maintains a high strength factor (6.00) and negligible displacement (0.30 mm), confirming its excellent stability. Sandy Limestone also shows improved parameters with a slightly increased strength factor (1.89) and moderate displacement (0.60 mm). While Shale's GSI improves to 30, its mechanical behavior remains weak, with the lowest strength factor (2.84) and the highest displacement (6.75 mm), implying poor stability. Overall, increasing GSI positively influences rock mass strength and reduces deformation, though the degree of improvement varies based on initial rock quality.

Table 9: *Analysis of numerical models for different geotechnical units (for 25% Decrease in GSI Values)*

S.No	Rock type	GSI	UCS MPa	Young Modulus MPa	Poisson ratio (V)	Generalized Hoek-Brown Parameters			Strength factor (F.O.S)		Total Displacement (mm)	
						mb	s	a	Crown	Sidewall	Crown	Sidewall
									After excavation		After excavation	
1	Limestone	48.75	57.2	22100	0.27	1.924	0.0034	0.506	3.47	1.26	0.30	0.06
2	Sandy Limestone	29.25	37.8	11400	0.30	1.159	0.0004	0.524	1.58	0.95	0.60	0.20
3	Shale	18	6.73	720	0.32	0.624	0.0001	0.55	2.53	0.95	6.75	2.25

Table 9 presents the results of numerical modeling for three rock types—Limestone, Sandy Limestone, and Shale—after a 25% decrease in Geological Strength Index (GSI), revealing a decline in rock mass quality and its effects on stability. With reduced GSI, the Hoek-Brown parameters (mb, s) drop significantly, indicating weaker rock mass strength. For Limestone, the strength factor decreases to 3.47 (from 6.00 in Table 7), while Sandy Limestone and Shale also show reduced strength factors (1.58 and 2.53, respectively). Despite these reductions, the total displacements remain nearly constant (e.g., 0.30 mm crown displacement for Limestone and 6.75 mm for Shale), suggesting that while strength is compromised, deformation may not always increase proportionally. Overall, lowering GSI degrades rock mass behavior, especially reducing stability margins, highlighting the critical role of rock quality in excavation safety assessments.

Table 10: *Analysis of numerical models for different geotechnical units (For 25% Increase in Poisson ratio values)*

S.No	Rock type	Poisson ratio (V)	UCS (MPa)	Young modulus (E) (Mpa)	GSI	Generalized Hoek -Brown Parameters			Strength factor (F.O.S)		Total Displacement (mm)	
						mb	s	a	Crown	Sidewall	Crown	Sidewall
									After excavation		After excavation	
1	Limestone	0.33	57.2	22100	65.00	3.438	0.0205	0.502	5.68	1.58	0.30	0.08
2	Sandy Limestone	0.37	37.8	11400	39.00	1.641	0.0011	0.512	1.89	1.26	0.65	0.20
3	Shale	0.40	6.73	720	24.00	0.773	0.0002	0.533	2.21	1.26	7.00	2.80

Table 11: *Analysis of numerical models for different geotechnical units (For 25% Increase in Poisson ratio values)*

S.No	Rock type	Poisson ratio (V)	UCS (MPa)	Young modulus (E) MPa	GSI	Generalized Hoek -Brown Parameters			Strength factor (F.O.S)		Total Displacement (mm)	
						mb	s	a	Crown	Sidewall	Crown	Sidewall
									After excavation		After excavation	
1	Limestone	0.20	57.2	22100	65	3.438	0.0205	0.502	5.68	1.58	0.30	0.06
2	Sandy Limestone	0.22	37.8	11400	39	1.641	0.0011	0.512	1.58	1.26	0.65	0.17
3	Shale	0.24	6.73	720	24	0.773	0.0002	0.533	3.47	1.26	6.75	1.50

Table 10 presents the results of numerical modeling for three rock types—Limestone, Sandy Limestone, and Shale—after a 25% increase in Poisson's ratio, illustrating how this change affects rock mass behavior and excavation stability. Poisson's ratio, which influences lateral deformation under stress, was adjusted to examine its impact on displacement and strength parameters. The modeling shows that with increased Poisson's ratio, the total displacement generally rises, especially in weaker rocks. For example, Shale, which has the highest Poisson's ratio (0.4) and lowest strength parameters (UCS = 6.73 MPa, GSI = 24), exhibits the greatest displacement (7.00 mm at the crown and 2.80 mm at the sidewall), indicating high deformability and potential instability. In contrast, Limestone, with a lower Poisson's ratio (0.3375) and higher strength (UCS = 57.2 MPa, GSI = 65), experiences minimal displacement (0.30 mm crown, 0.08 mm sidewall) and the highest strength factor (5.68 at the crown), reflecting good stability. Sandy Limestone falls between these two, with moderate displacement and strength. These results emphasize that increasing Poisson's ratio—especially in weak rock masses—can significantly amplify deformations, even if strength parameters remain unchanged, underlining the importance of accurately evaluating elastic properties in excavation design.

Table 11 presents the results of numerical modeling for three rock types—Limestone, Sandy Limestone, and Shale—after a 25% decrease in Poisson's ratio, highlighting how reductions in this elastic parameter influence rock mass behavior during excavation. Poisson's ratio affects the material's lateral deformation under axial stress, and decreasing it generally implies a stiffer, less laterally deformable response. In this analysis, despite the decrease in Poisson's ratio, total displacement values remain nearly unchanged when compared to the baseline (Table 5.8), indicating that reducing lateral strain does not significantly affect overall deformation in these rock types under the given conditions. For instance, Limestone, with the lowest Poisson's ratio of 0.2025 and high strength properties (UCS = 57.2 MPa, GSI = 65), maintains a very low crown displacement of 0.30 mm and a sidewall displacement of 0.06 mm, with a high strength factor of 5.68. Sandy Limestone and Shale, which have lower strength and stiffness, show higher displacements (0.65 mm and 6.75 mm at the crown, respectively), though these are still comparable to those observed in the baseline or increased Poisson's ratio cases. Interestingly, Shale shows a higher strength factor (3.47) in this scenario compared to Table 5.11, even though it retains the lowest UCS and GSI values, suggesting that reduced lateral deformation slightly improves stability margin .

Overall, the results indicate that while decreasing Poisson's ratio may not drastically affect displacements, it can contribute to slightly improved strength responses, especially in weaker rock masses like shale. This underscores the nuanced role of Poisson's ratio in excavation modeling and the importance of accurate elastic property estimation for reliable stability assessments.

Table 12: *Analysis of numerical models for different geotechnical units (For 25% Increase in USC Values)*

S.No	Rock type	UCS (MPa)	Young modulus (MPa)	GSI	Poisson ratio (V)	Generalized Hoek-Brown Parameters			Strength factor (F.O.S)		Total Displacement(mm)	
						mb	s	a	Crown	Sidewall	Crown	Sidewall
									After excavation		After excavation	
1	Limestone	71.50	22100	65	0.27	3.438	0.0205	0.502	6.00	1.58	0.30	0.06
2	Sandy Limestone	47.25	11400	39	0.30	1.641	0.0011	0.512	1.89	1.26	0.60	0.15
3	Shale	8.41	720	24	0.32	0.773	0.0002	0.533	2.84	1.26	6.75	1.50

Table 13: *Analysis of numerical models for different geotechnical units (For 25% Decrease in UCS Values)*

S.No	Rock type	UCS (MPa)	Young Modulus (MPa)	GSI	Poisson ratio (V)	Generalized Hoek-Brown Parameters			Strength factor (F.O.S)		Total Displacement(mm)	
						mb	s	a	Crown	Sidewall	Crown	Sidewall
									After excavation		After excavation	
1	Limestone	42.90	22100	65	0.27	3.438	0.0205	0.502	6.00	1.26	0.30	0.06
2	Sandy Limestone	28.35	11400	39	0.30	1.641	0.0011	0.512	1.58	0.95	0.65	0.20
3	Shale	5.05	720	24	0.32	0.773	0.0002	0.533	2.53	1.26	7.20	2.40

Table 12 shows the numerical modeling results for Limestone, Sandy Limestone, and Shale after a 25% increase in Uniaxial Compressive Strength (UCS), evaluating how improved rock strength affects excavation performance. With UCS increased to 71.5 MPa for Limestone, 47.25 MPa for Sandy Limestone, and 8.4125 MPa for Shale (while other parameters remain unchanged), the strength factors improve, especially for Shale, where the crown strength factor rises to 2.84 from previous lower values. Limestone maintains a high strength factor of 6.00, and Sandy Limestone shows a moderate value of 1.89.

Despite higher UCS, the total displacements remain nearly the same as before—e.g., Limestone shows 0.30 mm crown displacement, and Shale remains at 6.75 mm—indicating that deformation is more influenced by elastic properties (like Poisson's ratio and Young's modulus) than UCS alone. Overall, increasing UCS enhances stability margins, particularly in weaker rocks, but does not significantly reduce deformation without changes in stiffness or rock mass quality.

Table 13 presents the analysis of numerical models for different geotechnical units Limestone, Sandy Limestone, and Shale , after a 25% decrease in Uniaxial Compressive Strength (UCS). The UCS values have been reduced while other parameters like GSI and Young's modulus remain unchanged. Despite the reduction in UCS, the Generalized Hoek-Brown parameters (mb, s, a) are not affected (since they are primarily GSI-dependent), but the strength factors and displacements reveal significant behavioral changes. Limestone remains stable with a high strength factor (6.00) and minimal displacement (0.30 mm at crown). Sandy Limestone experiences a reduction in strength (factor 1.58) and an increase in displacement (0.65 mm), indicating moderate performance. Shale, being the weakest with the lowest UCS (5.05 MPa), shows increased deformation (7.20 mm crown displacement) and reduced strength factor (2.53), suggesting higher risk of instability. Overall, this analysis confirms that a decrease in UCS negatively affects the structural performance of rock masses, especially in weaker rock types like shale, leading to larger deformations and reduced stability.

Table 14 presents the effect of a 25% increase in Young's Modulus (E) on the numerical modeling of three rock types—Limestone, Sandy Limestone, and Shale—used in geotechnical analysis. Young's Modulus represents the stiffness of the rock; increasing it makes the rock more resistant to deformation. With this increase, all other parameters such as UCS, GSI, Poisson's ratio, and Hoek-Brown constants remain the same. As expected, the strength factors remain unchanged (since they depend more on UCS and GSI), but the total displacements are significantly reduced for all rock types. For example, crown displacement for Limestone drops to 0.25 mm (from 0.30 mm in Table 5.8), Sandy Limestone to 0.48 mm (from 0.60 mm), and Shale to 5.40 mm (from 6.75 mm). This shows that increasing stiffness leads to better deformation control, especially in relatively stronger rocks. However, weaker rocks like Shale still show high deformation despite improved stiffness, indicating that increasing Young's Modulus improves stability but cannot fully compensate for poor rock quality.

Table 14: *Analysis of numerical models for different geotechnical units (For 25% increase in Young Modulus Values)*

S.No	Rock type	Young modulus (E)	UCS	GSI	Poisson ratio V	Generalized Hoek -Brown Parameters			Strength factor (F.O.S)		Total Displacement(mm)	
						mb	s	a	Crown	Sidewall	Crown	Sidewall
									After excavation		After excavation	
1	Limestone	27265	57.2	65	0.27	3.438	0.0205	0.502	6.00	1.58	0.25	0.05
2	Sandy Limestone	14250	37.8	39	0.30	1.641	0.0011	0.512	1.58	1.26	0.48	0.16
3	Shale	900	6.73	24	0.32	0.773	0.0002	0.533	2.53	1.26	5.40	1.80

Table 15: *Analysis of numerical models for different geotechnical units (For 25% decrease in Young Modulus Values)*

S.No	Rock type	Young modulus (E) MPa	UCS MPa	GSI	Poisson ratio (V)	Generalized Hoek -Brown Parameters			Strength factor (F.O.S)		Total Displacement (mm)	
						mb	s	a	Crown	Sidewall	Crown	Sidewall
									After excavation		After excavation	
1.	Limestone	16575	57.2	65	0.27	3.438	0.0205	0.502	6.00	1.58	0.42	0.11
2	Sandy Limestone	8550	37.8	39	0.30	1.641	0.0011	0.512	1.58	1.26	0.78	0.26
3	Shale	540	6.73	24	0.32	0.773	0.0002	0.533	2.84	1.26	8.00	2.00

Table 15 illustrates the effect of a 25% decrease in Young's Modulus (E) on the geomechanical behavior of three rock types Limestone, Sandy Limestone, and Shale while keeping other parameters like UCS, GSI, and Hoek-Brown constants unchanged. A reduction in Young's Modulus leads to a significant increase in total displacement for all rocks, indicating greater deformation due to reduced stiffness. For instance, crown displacement for Limestone increases from 0.30 mm (in the original case) to 0.42 mm, for Sandy Limestone to 0.78 mm, and for Shale to 8.00 mm, which is the highest among all. Although the strength factors remain the same (since they depend on UCS and GSI), the overall structural behavior degrades as the rock becomes more deformable. This confirms that lower stiffness (E) compromises deformation control, making the rock mass more vulnerable to excessive movements during and after excavation, especially in weak rocks like Shale.

4. Sensitivity Analysis for different geological Parameters

In order to evaluate the effects of geological variability on tunnel stability, the Grey correlation Method was used to identify the most sensitive geological parameters. Sensitivity analysis was performed for all three geotechnical units to systematically examine the influence of individual geological parameters on the tunnel response. This approach provides a clear understanding of how variations in rock mass properties affect tunnel design requirements and overall stability, allowing the relative importance of each parameter to be assessed without altering the original modeling conditions. The different input parameters for the sensitivity analysis of all Geotechnical Units are presented in Table 16 ,17 and 18 respectively .

Table 16: *Input parameters for Sensitivity analysis of Limestone Unit*

S.No.	Geological Parameter	Actual Base values of Geological Parameters	25% Increase in values of Geological Parameters	25% Decrease in values Geological Parameters
1	GSI	65	81.25	48.75
	F.O.S	3.79	4.27	2.37
2	Poisson ratio	0.27	0.34	0.20
	F.O.S	3.79	3.63	3.63
3	UCS (MPa)	57.2	71.5	42.9
	F.O.S	3.79	3.79	3.63
4	Young Modulus (GPa)	22.10	27.27	16.58
	F.O.S	3.79	3.79	3.79

Table 17: *Input parameters for Sensitivity analysis of Sandy limestone Unit.*

S.No.	Geological Parameter	Actual Base values of Geological Parameters	25% Increase in values of Geological Parameters	25% Decrease in values Geological Parameters
1	GSI	39	48.75	29.25
	F.O.S	1.42	1.58	1.27
2	Poisson ratio	0.30	0.375	0.225
	F.O.S	1.42	1.58	1.42
3	UCS (MPa)	37.8	47.25	28.35
	F.O.S	1.42	1.58	1.27
4	Young Modulus (GPa)	11.40	14.25	8.55
	F.O.S	1.42	1.42	1.42

Table 18: *Input parameters for Sensitivity analysis of Shale Unit.*

S.No.	Geological Parameter	Actual Base values of Geological Parameters	25% Increase in values of Geological Parameters	25% Decrease in values of Geological Parameters
1	GSI	24	30	18
	F.O.S	2.05	2.05	1.74
2	Poisson ratio	0.32	0.40	0.24
	F.O.S	2.05	1.74	2.37
3	UCS (MPa)	6.73	8.41	5.05
	F.O.S	2.05	2.05	1.89
4	Young Modulus (GPa)	0.72	0.90	0.54
	F.O.	2.05	1.89	2.05

For the sake of brevity and time efficiency, only the sensitivity analysis procedures for limestone are presented in this paper, while the same methodology was consistently applied to the remaining geotechnical units.

Sensitivity analysis procedures for limestone are presented as follows:

Step # 1 Comparison matrix X is as follows:

$$X=\begin{bmatrix} X1 & 65 & 81.25 & 48.75 \\ X2 & 0.27 & 0.34 & 0.20 \\ X3 & 57.2 & 71.5 & 42.9 \\ X4 & 22.1 & 27.27 & 16.58 \end{bmatrix}$$

Step#2 Reference matrix Y is as follows:

$$Y=\begin{bmatrix} Y1 & 3.79 & 4.27 & 2.37 \\ Y2 & 3.79 & 3.63 & 3.63 \\ Y3 & 3.79 & 3.79 & 3.63 \\ Y4 & 3.79 & 3.79 & 3.79 \end{bmatrix}$$

Step #3 The dimensionless comparison matrix X' and the reference matrix Y', obtained through the interval relative value transformation method applied to the aforementioned matrices, are as follows:

$$X_i'(j)=\frac{X_i(j)-\min\limits_j X_i(j)}{\max\limits_j X_i(j)-\min\limits_j X_i(j)}$$

$$X'=\begin{bmatrix} X1' & 0.5 & 1 & 0 \\ X2' & 0.5 & 1 & 0 \\ X3' & 0.5 & 1 & 0 \\ X4' & 0.5 & 1 & 0 \end{bmatrix} \quad Y'=\begin{bmatrix} Y1' & 0.75 & 1 & 0 \\ Y2' & 1 & 0 & 0 \\ Y3' & 1 & 1 & 0 \\ Y4' & 0 & 0 & 0 \end{bmatrix}$$

Step#4 Difference sequence matrix is

$$=\begin{bmatrix} \mathbf{0.25} & \mathbf{0} & \mathbf{0} \\ \mathbf{0.5} & \mathbf{1} & \mathbf{0} \\ \mathbf{0.5} & \mathbf{0} & \mathbf{0} \\ \mathbf{0.5} & \mathbf{1} & \mathbf{0} \end{bmatrix}$$

Step#5 Grey correlation coefficient matric is

$$\gamma_{ij} = \frac{\Delta_{\min} + \zeta\Delta_{\max}}{\Delta_{ij} + \zeta\Delta_{\max}}$$

$$y = \begin{bmatrix} 0.667 & 1 & 1 \\ 0.5 & 0.33 & 1 \\ 0.5 & 1 & 1 \\ 0.5 & 0.33 & 1 \end{bmatrix}$$

The Grey Correlation Degree sequence is,
A=[0.89, 0.61, 0.83, 0.61]
The sensitivity analysis indicates that GSI (0.889) is the most sensitive parameter, followed by UCS (0.833). This suggests that variations in the Geological Strength Index have the greatest impact on the model's behavior, highlighting its critical role in geotechnical performance.
The grey correlation sequences for all the Geotechnical Units are presented in Table 19.

Table 19: Grey Correlation Degree sequence for all Geotechnical Units.

S.No	Geological Parmeter	Grey Correlation Degree		
		Limestone	Sandy Limestone	Shale
1	GSI	0.89	0.99	0.83
2	Poisson Ratio	0.61	0.84	0.54
3	Uni-axial Compressive Strength	0.83	0.99	0.83
4	Young Modulus	0.61	0.61	0.38

The sensitivity analysis revealed that GSI is the most influential parameter, followed by UCS, indicating that variations in these parameters significantly affect model behavior. This highlights the critical role of rock mass characterization, particularly the Geological Strength Index, in controlling geotechnical performance and stability.

5. Conclusion

This study confirms that geological variability plays a critical role in controlling the stability of the Kohat Tunnel. Numerical analysis using RS2 demonstrated that different geotechnical units respond differently to excavation due to variations in strength and deformation properties. Limestone exhibited comparatively better stability with lower deformations and higher strength, whereas sandy limestone and shale showed higher displacements and reduced stability, particularly in weaker zones. These results highlight that tunnel behavior is strongly governed by the mechanical characteristics and spatial variability of the surrounding rock mass.
The sensitivity analysis using the Grey Correlation Method further identified the most influential geological parameters affecting tunnel stability. The results show that the Geological Strength Index (GSI) and uniaxial compressive strength (UCS) have the strongest influence on the Factor of Safety, confirming that rock mass quality and strength are the primary controlling factors for tunnel stability. In contrast, Poisson's ratio and Young's modulus were found to primarily affect deformation behavior, with comparatively less influence on overall safety. The combined use of numerical modeling and sensitivity analysis provided a comprehensive framework for understanding and quantifying the effects of geological variability on tunnel performance.

Based on these findings, it is recommended that detailed geological and geomechanical characterization, particularly accurate determination of GSI and UCS, should be prioritized during site investigation and tunnel design. Design approaches should account for spatial geological variability, especially in weak or heterogeneous zones such as sandy limestone and shale, where additional support measures may be required. It is further recommended that sensitivity analysis be integrated into tunnel design procedures to identify critical controlling parameters and improve the reliability of stability assessments. Continuous monitoring during excavation, along with adaptive support design, is also essential to address uncertainties associated with changing ground conditions. Overall, the adopted methodology provides a reliable approach for evaluating tunnel stability in complex and heterogeneous rock masses and can be effectively applied to similar tunneling projects to enhance design safety, optimize support systems, and reduce geotechnical risks.

6. Acknowledgments

The authors acknowledge the Department of Mining Engineering, University of Engineering and Technology, Peshawar, for providing resources and technical support. Special thanks are extended to field engineers and laboratory staff for their assistance in data collection and testing.

References

[1] "Impacts of geological conditions on instability causes and mechanical behavior of large-scale tunnels: a case study from the Sichuan–Tibet highway, China | Bulletin of Engineering Geology and the Environment | Springer Nature Link." Accessed: Feb. 20, 2026. [Online]. Available: https://link.springer.com/article/10.1007/s10064-020-01796-w

[2] W. Zhang, X. Tang, W. Yang, J. Jiang, H. Zhang, and P. Li, "Review of tunnels and tunnelling under unfavorable geological conditions," Geol. J., vol. 59, no. 9, pp. 2668–2689, Sep. 2024, doi: 10.1002/gj.4937.

[3] "Assessment of a Concealed Karst Cave's Influence on Karst Tunnel Stability: A Case Study of the Huaguoshan Tunnel, China." Accessed: Feb. 20, 2026. [Online]. Available: https://www.mdpi.com/2071-1050/10/7/2132

[4] Q. Pan and D. Dias, "Three-dimensional face stability of a tunnel in weak rock masses subjected to seepage forces," Tunn. Undergr. Space Technol., vol. 71, pp. 555–566, Jan. 2018, doi: 10.1016/j.tust.2017.11.003.

[5] G.-H. Zhang, Y.-Y. Jiao, C.-X. Ma, H. Wang, L.-B. Chen, and Z.-C. Tang, "Alteration characteristics of granite contact zone and treatment measures for inrush hazards during tunnel construction – A case study," Eng. Geol., vol. 235, pp. 64–80, Mar. 2018, doi: 10.1016/j.enggeo.2018.01.022.

[6] W. Zhang, I. Somerville, G. Paneiro, X. Nong, M. Chwala, and W. Yang, "Design and construction of tunnels and tunnelling: Understanding the importance of geological conditions, landslide susceptibility and risk assessment," Geol. J., vol. 59, no. 9, pp. 2365–2370, 2024, doi: 10.1002/gj.5041.

[7] F. Wu et al., "Engineering behavior of soft rock tunnels in mountainous areas under multiple hazard inducers: a case study of the Jiuzhaigou-Mianyang Expressway," Bull. Eng. Geol. Environ., vol. 81, no. 8, p. 305, Jul. 2022, doi: 10.1007/s10064-022-02805-w.

[8] Z. Song, G. Shi, B. Zhao, K. Zhao, and J. Wang, "Study of the stability of tunnel construction based on double-heading advance construction method," *Adv. Mech. Eng.*, vol. 12, no. 1, p. 1687814019896964, Jan. 2020, doi: 10.1177/1687814019896964.

[9] "Stability analysis of existing tunnels under dynamic loads during excavation of new tunnels | Scientific Reports." Accessed: Feb. 20, 2026. [Online]. Available: https://www.nature.com/articles/s41598-024-81128-0

[10] "Review of tunnels and tunnelling under unfavourable geological conditions - Zhang - 2024 - Geological Journal - Wiley Online Library." Accessed: Feb. 20, 2026. [Online]. Available: https://onlinelibrary.wiley.com/doi/full/10.1002/gj.4937?casa_token=QdusRoDiDpMAAAAA%3AywoCHK8xCljBkEKQZFbH3jpwh8eTHx4F

ec5hD_wy41mE_4rRYxBr1MbFXgizUjhGz1DyzmQ099s6A7o
[11] "Comparative analysis and application of a new stability model for the tunnel face with Mogi-coulomb criterion | Geomechanics and Geophysics for Geo-Energy and Geo-Resources | Springer Nature Link." Accessed: Feb. 20, 2026. [Online]. Available: https://link.springer.com/article/10.1007/s40948-024-00914-2
[12] "Numerical Simulation Analysis of the Impact of Tunnel Construction on Aquifers in the Karst Regions of Southwestern China." Accessed: Feb. 20, 2026. [Online]. Available: https://www.mdpi.com/2073-4441/17/5/619
[13] D. Chen *et al.*, "An overview of ahead geological detection technologies in tunnels," *Eur. J. Remote Sens.*, vol. 58, no. 1, p. 2503240, Dec. 2025, doi: 10.1080/22797254.2025.2503240.
[14] B. Wu, W. Sun, G. Cai, and G. Meng, "Reliability analysis of shallow-buried tunnel construction adjacent to karst cave," *Comput. Geotech.*, vol. 145, p. 104673, May 2022, doi: 10.1016/j.compgeo.2022.104673.
[15] "Assessment of a Concealed Karst Cave's Influence on Karst Tunnel Stability: A Case Study of the Huaguoshan Tunnel, China." Accessed: Feb. 20, 2026. [Online]. Available: https://www.mdpi.com/2071-1050/10/7/2132
[16] "Analytical model for assessing collapse risk during mountain tunnel construction." Accessed: Feb. 20, 2026. [Online]. Available: https://cdnsciencepub.com/doi/abs/10.1139/cgj-2015-0064
[17] J. Chen, Z. Che, Q. Song, W. Song, X. Jiang, and K. Xu, "Comparative analysis and application of a new stability model for the tunnel face with Mogi-coulomb criterion," *Geomech. Geophys. Geo-Energy Geo-Resour.*, vol. 10, no. 1, p. 193, Dec. 2024, doi: 10.1007/s40948-024-00914-2.
[18] S. Zhang, A. Rodriguez-Dono, F. Song, and Z. Zhou, "Time-dependent tunnel deformations: Insights from in-situ tests and numerical analyses," *Tunn. Undergr. Space Technol.*, vol. 157, p. 106319, Mar. 2025, doi: 10.1016/j.tust.2024.106319.
[19] "A Rock Strength Prediction Model Utilizing Real-Time Data from Percussion–Rotary Drilling Measurements | Rock Mechanics and Rock Engineering | Springer Nature Link." Accessed: Feb. 20, 2026. [Online]. Available: https://link.springer.com/article/10.1007/s00603-025-04474-z
[20] M. S. Sabri, A. Jaiswal, A. K. Verma, and T. N. Singh, "Systematic Review of RMR, Q-System, and GSI in Tunnel Classification: Origin, Advancement, and Limitations," *Indian Geotech. J.*, Sep. 2025, doi: 10.1007/s40098-025-01401-5.
[21] "Land Data Assimilation: Harmonizing Theory and Data in Land Surface Process Studies - Li - 2024 - Reviews of Geophysics - Wiley Online Library." Accessed: Feb. 21, 2026. [Online]. Available: https://agupubs.onlinelibrary.wiley.com/doi/full/10.1029/2022RG000801
[22] H. Li, J. Feng, D. Su, X. Chen, and X. Guo, "A review of computational approaches for simulating fracturing mechanisms in layered rock formations," *Int. J. Coal Sci. Technol.*, vol. 12, no. 1, p. 99, Dec. 2025, doi: 10.1007/s40789-025-00836-8.
[23] Y. Liu, "Virtual Modelling Aided Phase Field Method of Fracture and Fatigue Analysis," Thesis, UNSW Sydney, 2025. doi: 10.26190/unsworks/31690.
[24] A. I. Kanlı, *Slope Engineering*. BoD – Books on Demand, 2021.
[25] C. Chen, B. Jiang, G. Guo, X. Wang, Z. Yan, and S. Wang, "Control Mechanism and Field Testing of Prestressed Support in Large Tunnel," *Geotech. Geol. Eng.*, vol. 43, no. 6, p. 297, Jul. 2025, doi: 10.1007/s10706-025-03259-z.
[26] "Analytical model for assessing collapse risk during mountain tunnel construction." Accessed: Feb. 21, 2026. [Online]. Available: https://cdnsciencepub.com/doi/abs/10.1139/cgj-2015-0064
[27] F. Wu, C. He, W. Yang, J. Nie, C. Yao, and F. Yang, "Mechanisms of interaction and influence zone partitioning of high geo-stress twin tunnels in complex mountainous regions," *Tunn. Undergr. Space Technol.*, vol. 159, p. 106462, May 2025, doi: 10.1016/j.tust.2025.106462.
[28] S. Sun, Z. Jiang, L. Li, and D. Qiu, "Model test and numerical verification of surrounding

rock stability of super-large-span and variable-section tunnels," *Tunn. Undergr. Space Technol.*, vol. 153, p. 106020, Nov. 2024, doi: 10.1016/j.tust.2024.106020.
[29] "Quantitative evaluation of geological uncertainty and its influence on tunnel structural performance using improved coupled Markov chain | Acta Geotechnica | Springer Nature Link." Accessed: Feb. 21, 2026. [Online]. Available: https://link.springer.com/article/10.1007/s11440-021-01287-6
[30] M. Stavropoulou, G. Exadaktylos, and G. Saratsis, "A Combined Three-Dimensional Geological-Geostatistical-Numerical Model of Underground Excavations in Rock," *Rock Mech. Rock Eng.*, vol. 40, no. 3, pp. 213–243, Jun. 2007, doi: 10.1007/s00603-006-0125-4.
[31] "Geomorphology of the Anthropocene in Mediterranean urban areas - Pierluigi Brandolini, Chiara Cappadonia, Gian Marco Luberti, Carlo Donadio, Leonidas Stamatopoulos, Cipriano Di Maggio, Francesco Faccini, Corrado Stanislao, Francesca Vergari, Guido Paliaga, Valerio Agnesi, Georgios Alevizos, Maurizio Del Monte, 2020." Accessed: Feb. 21, 2026. [Online]. Available: https://journals.sagepub.com/doi/abs/10.1177/0309133319881108
[32] V. Marinos, A. Goricki, and E. Malandrakis, "Determining the principles of tunnel support based on the engineering geological behaviour types: example of a tunnel in tectonically disturbed heterogeneous rock in Serbia," *Bull. Eng. Geol. Environ.*, vol. 78, no. 4, pp. 2887–2902, Jun. 2019, doi: 10.1007/s10064-018-1277-7.
[33] S. Shnorhokian and H. Mitri, "Quantifying the Influence of Variations in Rock Mass Properties on Stope Stability," *J. Sustain. Min.*, vol. 21, no. 4, p. 331, Nov. 2022, doi: 10.46873/2300-3960.1368.
[34] G. Anagnostou, A. Benardos, and V. P. Marinos, "Expanding Underground-Knowledge and Passion to Make a Positive Impact on the World," presented at the Proceedings of the ITA-AITES World Tunnel Congress 2023 (WTC 2023), 2023, pp. 12–18.
[35] Civil Engineering Programme, Department of Civil Engineering, Faculty of Engineering, Universiti Pertahanan Nasional Malaysia Kem Sungai Besi, 57000, Kuala Lumpur, Malaysia *et al.*, "Seismic Response of Tunnels Under Effect of Overburden Depth Using Simplified Pseudo-Static Analysis," *J. Kejuruter.*, vol. 37, no. 1, pp. 395–407, Jan. 2025, doi: 10.17576/jkukm-2025-37(1)-27.
[36] M. Stavropoulou, G. Exadaktylos, and G. Saratsis, "A Combined Three-Dimensional Geological-Geostatistical-Numerical Model of Underground Excavations in Rock," *Rock Mech. Rock Eng.*, vol. 40, no. 3, pp. 213–243, Jun. 2007, doi: 10.1007/s00603-006-0125-4.
[37] H. Rehman *et al.*, "Investigating Effect of Tunnel Size, Rock Mass Conditions, and In-Situ Stresses on Stability of Tunnels," *J. Min. Environ.*, vol. 13, no. 4, pp. 973–987, Oct. 2022, doi: 10.22044/jme.2022.12294.2231.